Desalination and Water Treatment
www.deswater.com

doi: 10.5004/dwt.2019.24264

158 (2019) 385–397
August

Remediation of methyl green dye from aqueous solution via adsorption and degradation using silica gel modified with hydrated zinc oxide catalyst

Nesrine M.R. Mahmoud[a,*], Medhat Mohamed El-Moselhy[b], Mishael. A. Alkhaldi[c]

[a]*Department of Basic Science, Deanship of Preparatory Year and Supporting Studies, Imam Abdulrahman Bin Faisal University, P.O. Box 1982, Dammam, Saudi Arabia, Tel. +20 1004698537/+966 541310405; email: nmmahmoud@iau.edu.sa*

[b]*Faculty of Science, Chemistry Department, Jazan University, Jazan, Saudi Arabia, email: medhatmohamed@yahoo.com*

[c]*Faculty of Science, Chemistry Department, Imam Abdulrahman Bin Faisal University (IAU), Saudi Arabia, email: mialkhaldi@iau.edu.sa*

Received 1 December 2018; Accepted 13 April 2019

ABSTRACT

The modification of silica via incorporation of hydrated zinc oxide (HZnO) with different loadings was achieved using wet precipitation technique. After drying at room temperature, the obtained samples calcined at 105°C and characterized using X-ray powder diffractometer, scanning electron microscopy, electron diffraction X-ray, transmission electron microscopy, Fourier transform infrared spectroscopy and BET. The data of characterizations indicated the well-distributed HZnO particles inside the silicate matrix with average particle size were lower than the detection limit of some characterization instruments. Furthermore, the modification with HZnO led to a noticeable decrease in BET surface area and the energy band gap due to the occupation of ZnO for interstitial positions inside the silicate matrix. The modified samples were successfully utilized in the adsorption and photocatalytic degradation of Methyl green dye as one of the cationic hazardous organic pollutants. The adsorption capacity of the sorbent catalyst was found to be 24.91 mg g^{-1}, while complete degradation of the (2×10^{-4} mol L^{-1}) dye was fulfilled in no more than 16 min. The influence of different experimental parameters as pH, temperature, concentration of the dye and dose of the catalyst was examined. The results obtained indicate that both adsorption and degradation of MG were a pH, dose and temperature dependent. The easiness of regeneration of the exhausted catalyst and its successive reuse confirmed remarkable economic efficiency.

Keywords: Silica gel; HZnO modification; Adsorption; Photodegradation; Methyl green

1. Introduction

Colors resulting from dyes and pigments widely affect people's lives all over the world. Organic dyes are used in many fields as in the pharmaceutical, textile, food, cosmetics, paint, plastics, ink, photography, electroplating and paper industries [1]. However, organic dyes are highly noxious, mutagenic and may significantly affect the photosynthetic activity. Dyes are known to have complex aromatic structures which increase their stability and make them more difficult to biodegrade [2].

Adsorption is undoubtedly the most important of the physicochemical processes responsible for the discharging of organic substances, especially dyes in the aqueous environment [3]. The wide use of adsorption is due to low costs, easiness of operation, and being a relatively fast process [1]. However, adsorption is not effective in the complete elimination of the dyes. This is not the only drawback of adsorption especially when dealing with toxic materials but also adsorption might be a method for only accumulating

* Corresponding author.

and transferring the pollutant from the aqueous state to the adsorbent surface. Also, saturation of the adsorption sites acquires replacing adsorbents continuously. The used adsorbents should be regenerated for recycling, which, if applicable usually needs thermal energy [4] which decreases the economic efficiency of the adsorption process. Therefore, various advanced oxidation processes (AOPs) have been focussed by researchers in the last decades in order to support the oxidation of stubborn pollutants, as it is considered a destructive technique through the creation of highly reactive hydroxyl radicals (•OH) [5].

Semiconductors such as ZnO, TiO_2, CdSe and SnO_2 have captivated focus due to their versatile applications in the photocatalysis, photoluminescence and optoelectronic industries [6]. Among these semiconductors, ZnO has attracted lots of attention in photocatalytic applications due to its high photosensitivity and stability in degrading miscellaneous hazardous materials [7]. Synthesis of ZnO as nanoparticles improves its performance in any surface-associated application including heterogeneous catalysis. However, the particle size is not the only influence improving performance but also their structural uniformity, total surface area and porosity [8].

However, two important problems arise due to aggregation of the nanoparticles as a result of the large surface-to-volume ratio of particles which is always accompanied with considerable increases in the surface free energy [9]. The other problem is the separation of the photocatalyst from the treated suspension as it represents an obstacle toward the practical application [4]. In order to resolve these problems, the photocatalytic nanoparticles (e.g., ZnO) can be immobilized on the high surface area supports which appears to be a successful approach.

Different materials such as perlite, silica, fly ash, zeolites activated carbons and clays have been used for this purpose [5]. Although silica is known to be an inert material it can be doped with metal ions both in the silica matrix as well as on the surface or may be functionalized with organic molecules via covalent linkages [9]. Silica gel can be used as a bottom bed in order to obtain granular photocatalyst adsorbent with high physical strength in water, scratch-proof characteristics, chemical stability, dynamic resistance, durability in addition to low cost and the high surface area [10]. Besides, silica-coated nanoparticles are easy to centrifuge during preparation. These properties make silica a convenient material for metal oxide shielding and functionalization [11]. In addition, modification by such transition metal oxides is considered one of the most efficient methods for reducing electron–hole recombination [5] and can be regenerated if required [10].

In the current study, we establish a novel, bi-functional material which gathers the advantages of efficient adsorbents and high degradation power of photocatalysts. The photocatalyst adsorbent Si–HZnO possesses salient characteristics of large surface area nanoparticles, chemical stability, durability and low cost. These distinguished characteristics allow for the rapid elimination of the stubborn organic dyes such as methyl green (MG), and for the photocatalytic regeneration of saturated adsorbents under light conditions. Moreover, the loaded ZnO is strongly linked into the silica matrix which prevents its dissolution during the degradation reaction.

2. Materials and methods

2.1. Materials

Methyl Green dye (MG) with the molecular formula $C_{27}H_{35}Cl_2N_3{\cdot}ZnCl_2$ and 98% purity (C.I. 42590), sodium hydroxide, zinc nitrate, H_2O_2 (30%) and hydrochloric acid were purchased from Merck (USA). High-purity silica gel (pore size 60 Å); (mesh size 70–230) was purchased from Sigma-Aldrich (USA). AR grade was used as received without further purification.

2.2. Synthesis of Si–HZnO

50 g of pure silica gel was mixed by shaking with 5% (wt.) NaOH for 10 min. The mixture was washed with distilled water several times. A portion of 0.5 g zinc nitrate solution was added to the washed mixture, dried at 105°C for 4 h [10–12]. This preparation has been given the name Si–HZnO-I. The same procedure was repeated four times using different doses of $ZnNO_3{\cdot}2H_2O$ (1, 1.5, 2 and 2.5 g) to prepare another four different loadings of hydrated zinc oxide resulting in a series of catalysts which will be treated as Si–HZnO-II till Si–HZnO-V.

2.3. Catalyst characterization

2.3.1. Morphological characterization of Si–HZnO

Scanning electron microscopy (SEM) and transmission electron microscopy (TEM) are used to study the morphological features and structure of the micro and nanomaterials. In this study, the morphology and arrangement of the synthesized nanoparticles were performed using SEM (FEI, ISPECT S50, Czech Republic). SEM was operated at 20 kV and working distance around 10 mm. The samples were mounted on a metallic stub with a double-sided adhesive tape. For TEM, the synthesized samples were dispersed in ethanol, sonicated for 5 min and deposited onto TEM grids having a carbon support film. TEM grids were mounted into the TEM upon evaporation of water in air. A TEM, FEI, Morgagni 268, Czech Republic at 80 kV was used to record the images of the specimens.

Electron diffraction X-ray (EDX) analyses were performed using energy dispersive X-ray fluorescence spectrometer, EDX-8000 (Shimadzu, USA), and with an X-ray tube with Rh target voltage/current 4–50 kV/1 to 1,000 μA.

2.3.2. Structural characterization

The crystalline structure of the developed phases was assessed by Shimadzu (USA) X-ray powder diffractometer (XRD) with Cu Kα radiation (λ = 1.5418 Å) at a scanning speed of 0.2 S. The applied operating voltage and current were 40 kV and 40 mA, respectively.

The Brunauer–Emmett–Teller (BET) surface area was determined on the basis of the volumetric nitrogen adsorption on a Nova 1200 of the Quantachrome Corporation, Florida, USA. The surface area, total pore volume and micropore volume were determined by multi-point BET, *t*-plot and DR (Dubinin–Radushkevich), respectively.

Zeta potential was measured using the Zetasizer (Malvern Instruments, UK) at 633 nm and a 173° backscattering angle

at a fixed refractive index of the respective formulations to assess nanoparticles stability.

Solid spec-3700-UV spectrophotometer (Shimadzu, USA) was used at a resolution of 64 nm. Solid disc prepared to identify bonding energy gap of each silica gel modified catalyst.

Fourier transform infrared (FTIR) spectra were recorded using Shimadzu (USA). The spectra were taken at 4.0 cm^{-1} resolution. 64 scans were accumulated to obtain a reasonable signal to noise ratio. The FTIR spectra were obtained in the wave number range 400–4,000 cm^{-1}.

2.4. Determination of Zn Content and MG concentration

2.4.1. Measurements of MG concentration and TOC in the synthetic wastewater

Determination of MG was performed by measuring the absorbance water containing MG samples at λ_{max} = 631 nm using a UV–Vis Double PC 8 Auto Cell Scanning Spectrophotometer UV–Vis double beam (Model UVD-3000).

Total organic carbon (TOC), total carbon (TC), inorganic carbon (IC), total nitrogen (TN) was monitored using a Shimadzu TOC-L analyzer, USA.

2.4.2. Measurements of Zn content loaded on silica

Total loaded Zn was carried out using Shimadzu (USA) atomic absorption spectrophotometer with graphite furnace accessories (Model AA-7000). The zinc content of silica was estimated through the treatment of 0.1 g of all samples with 10 mL concentrated (2 M) HCl to leach out the precipitated zinc hydroxide before analysis with AAS.

The analysis carried out for the determination of loaded zinc ions indicated 0.98 to 6.18 mg Zn/g Si in the five different loadings.

2.5. Adsorption studies

Adsorption measurement was determined by batch experiments by mixing 0.15 g of Si–HZnO-II with 100 mL solution of methyl green of 6, 12, 18, 24, 36, 45 and 70 mg L^{-1} concentrations followed by mechanical stirring using a shaker incubator at 200 rpm. No pH adjustment was done in any of the cases. Mixtures were taken from the shaker at appropriate time intervals and the concentration of the methyl green solution left was estimated. The amount of MG adsorbed at equilibrium per unit mass of modified, q_e, was calculated by:

$$q_e = \frac{C_e - C_0}{m} \times V \quad (1)$$

where V is the volume of MG solution in L; C_0 and C_e are the initial and the equilibrium concentrations in mg L^{-1}, respectively; and m is the mass of adsorbent in g. Kinetic experiments were performed by placing 0.15 g sorbent into flasks containing 100 mL of MG solution (70, 24 and 12 mg L^{-1}) at 20°C and 200 rpm shaking speed. At suitable time intervals, 5 mL of sample was withdrawn and the amount of MG was determined by the spectrophotometer.

2.6. Photocatalytic degradation test

All batch experiments for MG photodegradation by the synthesized photocatalyst Si–HZnO was conducted with different doses of the catalyst suspended in synthesized MG dye solution, under permanent mechanical stirring and a constant flow of bubbled air, subjected to UV irradiation by immersing 6 W Hg lamp (254 nm) within the photoreactor, where a total radiant flux (20 $MWcm^2$) was applied. The radiation flux was measured with a UV radiometer (Digital, UVX, 36). All measurements were performed at 25°C. At different time intervals, an aliquot was withdrawn which was, subsequently, filtered through 0.45 μm (Millipore) syringe filter. Absorption spectra were recorded, and the rate of decolorization was observed in terms of change in intensity at 631 λ_{max} of the MG dyes. Similar experiments were carried out by varying the pH of the solution (pH 3–9), the initial concentration of MG dye (50 mg L^{-1}), and the catalyst dose 1.5 g/100 mL.

3. Results and discussion

3.1. Si–HZnO characterization

3.1.1. X-ray diffractometer

X-ray diffraction patterns of the parent silica gel and the ones modified with different Zn contents are shown in Fig. 1. An amorphous structure of the synthesized Si–HZnO samples is obtained as indicated from the different patterns with

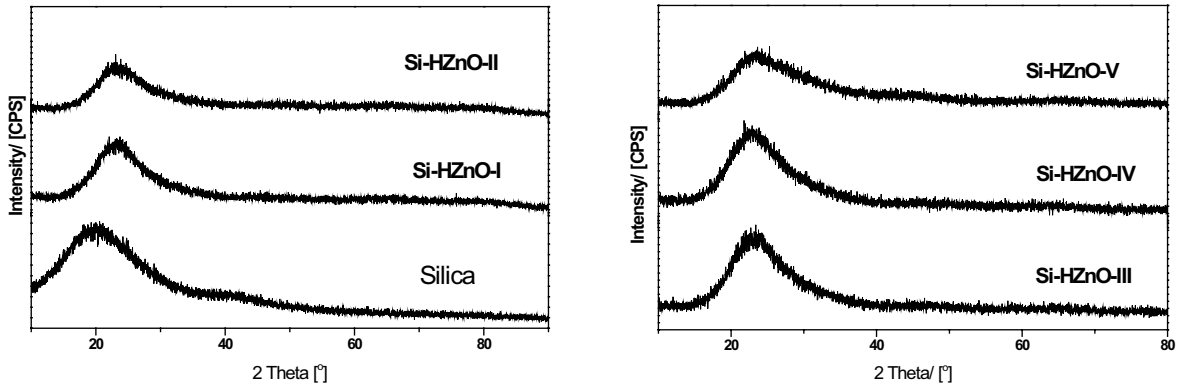

Fig. 1. XRD patterns of silica gel and modified Si–HZnO samples.

no diffraction lines. The obstruction to detect ZnO species may be assumed to either of, the lower amounts of Zn residing on the surface which is below the detection limit of the instrument or may be attributed due to occupation of ZnO an interstitial positions inside the matrix of the silicate [10].

3.1.2. Fourier transform infrared

Fig. 2 elucidates the FTIR spectra of Si–HZnO samples containing different ratios of Zn compared with the parent silica gel. The bands at 992, 854 and 412 cm^{-1} are observed in the parent silica gel which can be attributed to the different tetrahedral framework atoms vibrations in the silicate structure [10]. In general, the IR bands at 412, 854 and 992 cm^{-1} corresponds to bending modes of Si–O–Si linkage symmetric stretching and asymmetric stretching, respectively [13]. While for optimal Si–HZnO modified samples, appearance of a new peak at 472 cm^{-1} in the modified sample no. 3 with increasing intensities in samples 4 and 5 besides the mentioned bands assigned to the formation of a zinc oxide phase on silica nanoparticles [14]. The strong absorption band emerged at 428 cm^{-1} can be allocated due to Zn–O stretching mode of ZnO nanoparticles [15]. Furthermore, initial bands in silica nanoparticles at 992 cm^{-1} disappeared after introducing the ZnO into the silicate matrix, the intensity of another band at 854 shifted and gets more broader indicating the formation of metal oxide on silica nanoparticles [16].

3.1.3. Scanning electron microscopy

Fig. 3a illustrates the images resulting from SEM. It elucidates the morphology and recommends the particle size of the synthesized catalyst. The images show the HZnO particles scattered randomly all over the rough surface of the silica. The data indicated that reasonable portions of the loaded HZnO exist on the surface; however, the rest is hidden. This observation is reinforced by the EDX data, revealing high ratio of Zn recorded on the surface. The size of particles determined ranged from 22 to 39 nm. The particles are being granular with no other shapes [17].

3.1.4. Transmission electron microscopy

Fig. 3b illustrates the morphologies of Si–HZnO crystallites and particles investigated by TEM. The light spots and areas in the obtained image represent the silica surface; however, the dim ones represent the loaded ZnO nanoparticles dispersed within the silica matrix. This can suggest that ZnO

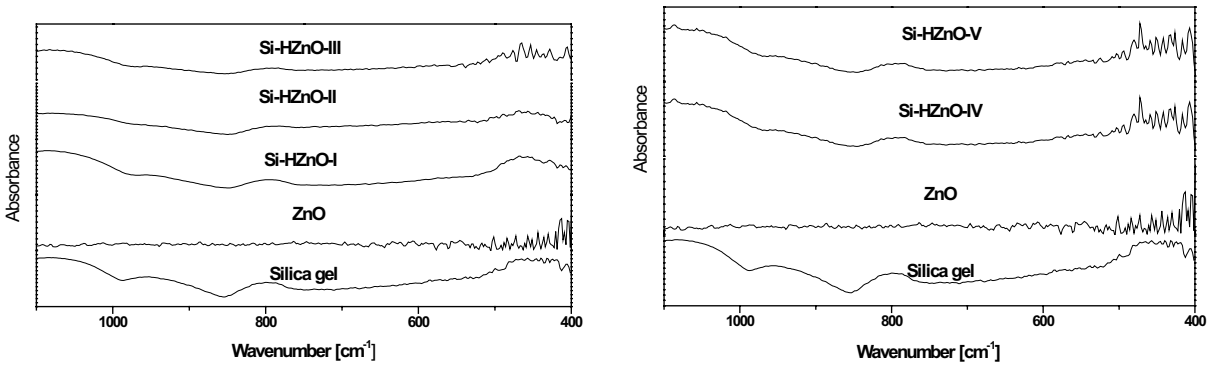

Fig. 2. FTIR of silica gel, ZnO and modified Si–HZnO samples.

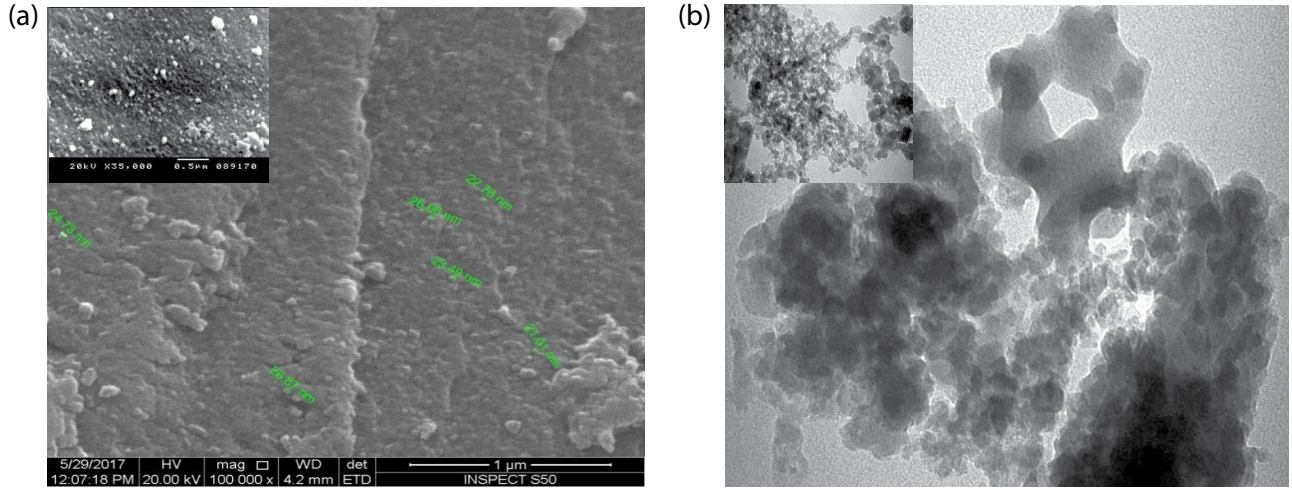

Fig. 3. (a) SEM and (b) TEM images of modified Si–HZnO at different magnification.

remarkably occupies inside the silicate matrix with a lower particle size that support its un-detection by XRD. The average particle diameter was found to be 10 nm, even though particles in the range of 6.5–23.5 nm are obviously scattered on the surface.

3.1.5. Electron diffraction X-ray

The EDX patterns of the synthesized silica samples modified with HZnO is shown in Fig. 4. The presence of Zn was quantitatively approved by energy dispersive X-ray analysis. The percentage of Zn varies from 1.14 to 20.1 in the different modified samples from Si–HZnO-I till Si–HZnO-V. The data indicated that only few moieties of the loaded zinc exist on the surface of the samples Si–HZnO-I and Si–HZnO-II; however, loaded Zinc increased on the surface from sample Si–HZnO-III till sample Si–HZnO-V.

The detected weight percentages are relatively consistent with the starting compositions of zinc cations introduced into the silica gel.

3.1.6. Energy band gap

The band gap of Si–HZnO-II sample was calculated by using formula $E = hc/\lambda$, where h is the Plank's constant, c is the velocity of light and λ is the wavelength. A band gap narrowing was exhibited, it was found to be 2.74 eV. The observed difference between the calculated band gap and the reported values [18] arises from embedding of the ZnO nanoparticles into the interstitial positions of the silicate matrix [19].

3.1.7. Surface area texturing

Measuring surface properties for the synthesized samples within P/P_0 range between 0.4 and 0.6 [20] indicate that the obtained adsorption/desorption hysteresis loops are of type II and differs only in the upward deviation at the start of the isotherm (Fig. 5). The presence of upward deviation could reflect the nature of pores and the effect of loading process. Going through the isotherm, the flat region in the middle of the isotherm was considered as a sign of the monolayer formation that was formed due to the capillary condensation of nitrogen inside the micropores. Furthermore, multilayer formation occurred at medium pressure levels, while at higher ones capillary condensation is formed. Additional loading of HZnO into silica gel as in Si–HZnO-V sample revealed type IV isotherm characterized by a long upward deviation hysteresis loop (at P/P_0 = 0.32–0.84). On the other hand, at lower pressure the sharp rise in the knee indicates a high surface area as depicted in Table 1.

3.1.8. Zeta-potential of Si–HZnO

Zeta potential of the synthesized catalyst is studied to measure the magnitude of the electrostatic or charge repulsion/attraction between particles of the catalyst. The results of zeta potentials against pH values are illustrated in Fig. 6. The pH_{ZPC} of the catalyst was recorded at 4.8 and 5. From the determined values, it appears that the catalyst surface is negatively charged in a pH ranging from 3.0 to 9.0 which is considered a wide range with the exception of the narrow range of 4.8 < pH < 5 in which the catalyst surface appears to be positively charged. The high negative zeta potential (surface charge density) values measured may indicate greater stability in dispersion and smaller probability of flocculation which may be attributed to repulsive force between particles [21]. These results recommend that adsorption of cationic dyes is easier on the synthesized catalyst [22]. As MG has cationic polar groups, they can be attracted to the adsorbent which carries a negative charge. Therefore, the electrostatic attraction forces have been involved in the adsorption mechanism [23].

3.2. Adsorption and catalytic activity of Si–HZnO

To have a full conception of the degradation process, the adsorption behavior of MG using the synthesized Si–HZnO was investigated at different experimental conditions to determine adsorption capacity of the catalyst as well as its surface properties.

3.2.1. Adsorption isotherm

The nature of the adsorption process could be suggested by studying the adsorption isotherm. Various isotherm

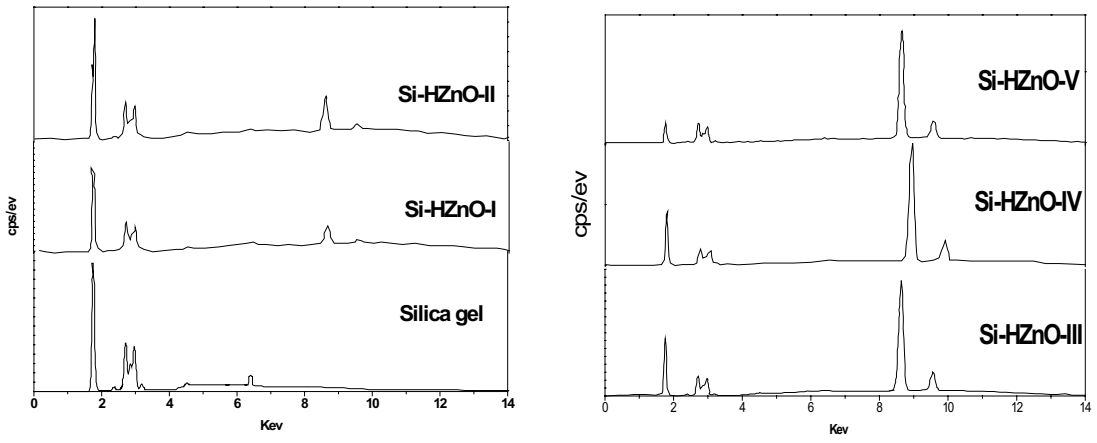

Fig. 4. EDX mapping of silica gel and modified samples.

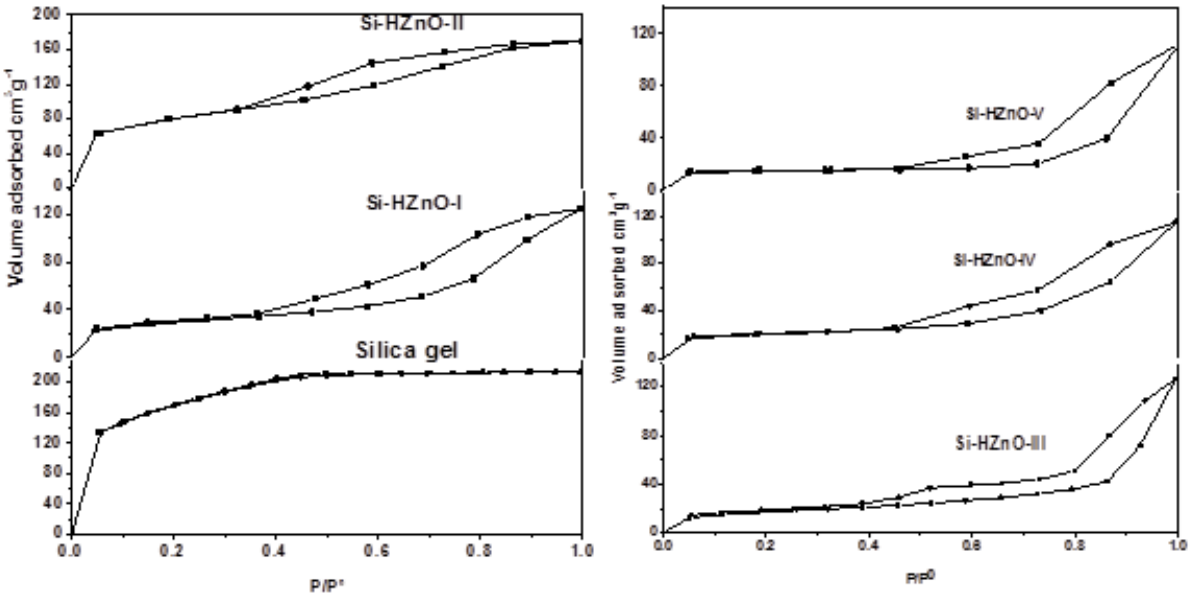

Fig. 5. Nitrogen adsorption–desorption isotherms of samples.

Table 1
Changes in surface areas and pore characteristics of silica with reference to zinc loading

Sample	Specific surface area (BET) $m^2\ g^{-1}$	Total pore volume $cm^3\ g^{-1}$	Average pore diameter Å
Silica parent	587.4	0.256	17.4
Si–HZnO-I	311.4	0.133	17.1
Si–HZnO-II	297.2	0.128	17.3
Si–HZnO-III	295.3	0.127	17.1
Si–HZnO-IV	170.3	0.073	17.2

equations have been described, and three major isotherms, the Langmuir, Freundlich and Temkin isotherms [24], are applied to test the experimental data.

3.2.1.1. Langmuir isotherm

The Langmuir adsorption isotherm has been successfully applied for a wide variety of adsorption processes of cationic dyes [25]. It assumes that adsorption occurred to homogeneous sites in the absorbent [26]. It can be exhibited as follows:

$$q_e = \frac{q_m K_L C_e}{1 + K_L C_e} \tag{2}$$

where q_m is the adsorption capacity representing the formation of a complete monolayer and K_L is the Langmuir constant.

The Langmuir isotherm model can also be given in a linear form as follows:

$$\frac{C_e}{q_e} = \frac{1}{q_m} \times C_e + \frac{1}{q_m K_L} \tag{3}$$

The Langmuir isotherm is assessed to fit the experimental data; a linear plot is observed in Fig. 7. Langmuir constants

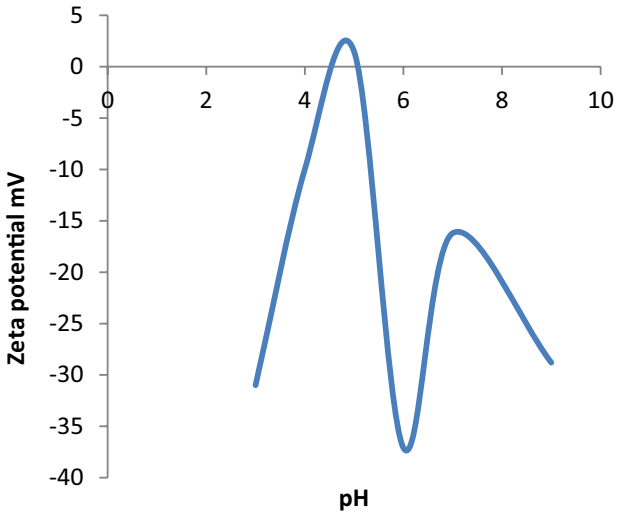

Fig. 6. Zeta potential values against pH values of Si–HZnO-II.

(q_m and K_L) can be calculated from the slope and intercept of the plot and are presented in Table 2. Adsorption capacity (q_m) was found to be 24.91 mg g^{-1} for the synthesized sorbent, Si–HZnO. Fitting the experimental results with Langmuir isotherm recommends monolayer adsorption.

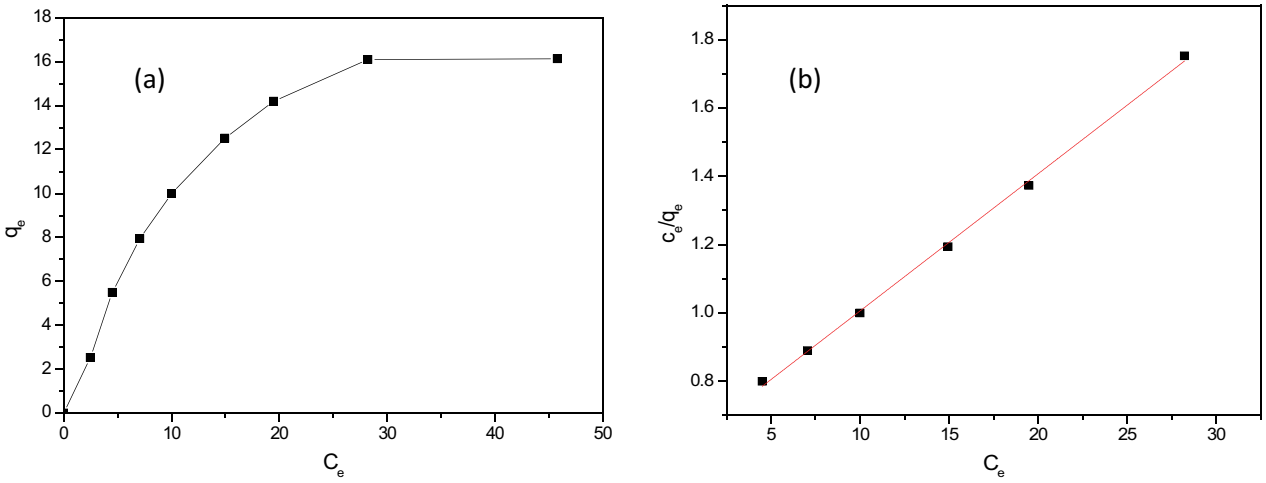

Fig. 7. (a) Langmuir isotherm for MG adsorption and (b) Langmuir isotherm for MG adsorption using linearized equation.

Table 2
Isotherm parameters and correlation coefficients calculated by various adsorption models onto 0.15 g of Si–HZnO-II in 100 mL of (36 mg L^{-1}) dye, at room temperature

Isotherm	Parameters	
Langmuir	q_m (mg g^{-1})	24.91
	K_L (L mg^{-1})	0.07
	R_L	0.284
	R^2	0.992
Freundlich	K_f (mg g^{-1})(mg $L)^{-1/n}$	1.99
	n	1.59
	R^2	0.899
Temkin	A (L g^{-1})	0.599
	b (kJ mol^{-1})	0.4275
	R^2	0.998

To test the favorability of adsorption, a dimensionless constant called separation factor (R_L) was also calculated [26].

$$R_L = \frac{1}{1 + K_L C_0} \tag{4}$$

where K_L is the Langmuir isotherm constant and C_0 is the initial metal ion concentration (mg L^{-1}). The separation factor is a parameter which explains the isotherm as follows: $R_L > 1$ unfavorable, $0 < R_L < 1$ favorable, $R_L = 0$ irreversible, $R_L = 1$ for linear adsorption [27].

The value of R_L for the present synthesized sorbent is in the range of 0–1, which confirms favorable uptake of MG by the Si–HZnO-II. This recommends that the equilibrium isotherms reasonably fitted well by the Langmuir isotherm model [28]. The adsorption process is considered to be a monolayer adsorption onto a surface with finite number of identical sites, which are homogeneously dispersed over the adsorbent surface [29].

3.2.1.2. Freundlich isotherm

It is an empirical representation for adsorption onto heterogeneous surface, which is in the form as follows:

$$K_F = q_e C_e^{1/n} \tag{5}$$

The linearized form of the Freundlich isotherm model is given as follows: [30]

$$\log q_e = \log K_f + \frac{1}{n} \log C_e \tag{6}$$

where K_f is the Freundlich equilibrium constant ([mg g^{-1}] [mg $L^{-1}]^{-1/n}$) which expresses the capacity of the adsorption and n indicates the intensity of adsorption, that is, the degree of nonlinearity between MG concentrations. A plot of log q_e against log C_e results in a linear function, where $1/n$ and K_f can be calculated from the slope and the intercept; the results are summarized in Table 2. The value of $1/n$ gives an idea about the intensity of the adsorption. Favorable adsorption is reported for $0.1 < 1/n < 1$ which is indicated in the adsorption of MG over the synthesized sorbent Si–HZnO-II [31]. The correlation coefficient R^2 showed compatibility of the data obtained with Langmuir more than Freundlich.

3.2.1.3. Temkin isotherm

This isotherm assumes that the fall in heat of adsorption of all molecules in a layer is linear rather than logarithmic, as indicated in Freundlich isotherm [24]. According to the Temkin isotherm, heat of adsorption would decrease linearly with increasing surface coverage due to some indirect adsorbate/adsorbent interactions [32].

The linearized form of the Temkin isotherm is given below [33]:

$$q_e = \left(\frac{RT}{b}\right) \ln A + \left(\frac{RT}{b}\right) \ln C_e \tag{7}$$

where A is the Temkin isotherm equilibrium binding constant (L g^{-1}), b is the Temkin constant related to the heat of sorption (kJ mol^{-1}), R is the gas constant (0.0083 kJ mol^{-1} K^{-1}), and T is the absolute temperature (K). Therefore, plotting q_e vs. lnC_e, and the values of both constants A and b were calculated from slope and intercept shown in Table 3. Typical bonding energy range for ion-exchange mechanism is reported to be in the range of 8–16 kJ mol^{-1} while physisorption processes are reported to have adsorption energies less than −40 kJ mol^{-1} [24]. Value of b = 0.4275 kJ mol^{-1} calculated in the current study assumed that the adsorption process is likely to involve both chemisorption and physisorption [34].

The adsorption of MG on the adsorbent Si–HZnO was adequately described by the Langmuir isotherm, recommended by the high R^2 values. It confirms the monolayer adsorption of MG onto Si–HZnO surface [35]. The maximum adsorption capacity (q_m) calculated using the Langmuir isotherm was 24.91 mg g^{-1}. The experimental data also fitted satisfactorily to the Temkin isotherm model, which assumes a linear decrease in the heat of adsorption of all the molecules in the layer. This decrease may be attributed to the MG molecules repulsion and homogeneous distribution of MG into silicate matrix [36].

3.2.2. Adsorption kinetics

The investigation of reaction kinetics is of important concern to get an idea about the behavior of both adsorbent and adsorbate and interaction of both of them.

The experimental data have been analyzed by the kinetic models, such as pseudo-first-order and pseudo-second-order. To predict and select the optimum conditions for the dye removal processes, full data on the kinetics of the dye uptake is required [20]. The Lagergren pseudo-first-order model [28] described the adsorption kinetic data.

$$\log\left(q_e - q_t\right) = \frac{\log\left(q_e\right) \times K_1}{2.303} \tag{8}$$

log ($q_e - q_t$) is plotted vs. t, in which the slope and intercept show the values of K_1 (min^{-1}) and q_e, respectively. Moreover, the correlation coefficient R^2 is almost low for most adsorption data presented in Table 3.

The pseudo-second-order model can be expressed as follows:

$$\frac{t}{q_t} = \frac{1}{K_2 q_e^2} + \frac{t}{q_e} \tag{9}$$

where K_2 is the equilibrium rate constant of pseudo-second-order adsorption (g mg^{-1} min^{-1}). Values of q_e and K_2 were calculated from the intercepts and slopes of the linear plot of t/q_t against t. The regression coefficients R^2 are found to be greater than 0.991 among the concentrations used, and the calculated maximum adsorption capacity values of q_e, which are relatively close to the experimental values. Thus, the adsorption of MG onto Si–HZnO indicates that the pseudo-second-order model best fitted to the kinetic data. The values of K_2 and q_e calculated are recorded in Table 3.

3.2.3. Thermodynamic parameters

The thermodynamic parameters were calculated from the experimental data obtained at different temperatures. The free energy change ($\Delta G°$) of the adsorption can be given as follows:

$$\Delta G^{\circ} = -RT \ln K_L \tag{10}$$

$\Delta G°$ is the Gibbs free energy of adsorption (kJ mol^{-1}), R is the gas constant (8.314 Jmol^{-1} K^{-1}), and K_L is the equilibrium constant depending on the temperature. Plotting ln K with 1/T showed a linear variation. $\Delta H°$ and $\Delta S°$ were obtained from the slope and intercept of the linear variation of ln K with 1/T. The thermodynamic parameters ΔH, and ΔS are calculated according to the Van't Hoff equation [37] as follows:

$$\ln K = \frac{-\Delta H}{R} \times \frac{1}{T} + \frac{\Delta S}{R} \tag{11}$$

As several dye effluents are produced at relatively high temperatures; the temperature can be a determining factor in the real application of Si–HZnO. Temperature is a sign of the adsorption nature, whether it is an exothermic or endothermic process [38]. Increasing the value of K as illustrated in Table 4 indicates that the adsorption rate of MG is increased upon rising the temperature [39]. The nonspontaneous behavior of MG adsorption could be assumed from the positive values of $\Delta G°$ recorded at different temperatures. The endothermic nature of adsorption is confirmed by positive value of ΔH which is consistent with previous studies on the MG adsorption [28]. The high value of ΔH 79.08 kJ mol^{-1} recommends chemisorption which may be supported by increasing the rate of adsorption upon rising the temperature. The positive value of ΔS indicates increasing randomness reflecting the affinity of the Si–HZnO toward methyl green species in

Table 3
Adsorption kinetic parameters at different initial concentrations onto 0.15 g of Si–HZnO-II in 100 mL of the MG dye at room temperature

Concentration (mg L^{-1})	Pseudo-first-order			Pseudo-second-order			
	K_1	q_e	R^2	K_2	q_e	h	R^2
12.0	0.209	7.298	0.967	0.031	8.511	2.246	0.991
24.0	0.288	9.42	0.988	0.039	10.94	4.668	0.993
70.0	0.411	16.129	0.991	0.003	46.08	6.370	0.995

Table 4
Thermodynamic parameters for adsorption of MG on Si–HZnO-II

	Thermodynamic parameters					
Temperature	K_L (L mg^{-1})	lnK_L	$\Delta G°$ (kJ mol^{-1})	$\Delta H°$ (kJ mol^{-1})	$\Delta S°$ (J K^{-1} mol^{-1})	R^2
288	0.0236	–3.746	9.31	79.08	243.192	0.998
293	0.0382	–3.264	8.08			
303	0.119	–2.128	5.358			

aqueous solutions and may suggest some structural changes in adsorbents [40] under the studied conditions.

3.2.4. MG photolysis

Fig. 8a illustrates the obtained UV–Vis spectra of the MG solution against the irradiation time. The main absorbance peak at a wavelength of 631 nm was attributed to the chromophore quinonoid to which this class of dyes belongs. The band decreased during the process of irradiation, indicating the decomposition of methyl green and the decolorization of the solution.

The stability of MG toward photodegradation using UV irradiation was investigated at different concentrations of the dye. Different degradation rates are revealed from the data indicating that the concentration of MG applied is a key factor in the degradation process. It is obvious from the data that the rate of degradation increases upon decreasing the dye concentration, as depicted in Fig. 8b.

To have a comprehensive idea about the reactivity of the synthesized catalyst in the degradation process of organic dyes in the bench scale, its catalytic activity was tested by changing the experimental conditions. Fig. 8c elucidates the degradation of MG dye in the absence and presence of the synthesized catalyst. About 90% degradation of MG dye of (120 mg L^{-1}) depleted more than 35 min in the presence of UV/H_2O_2 only as specified in Fig. 8c. The addition of Si–HZnO to, UV/H_2O_2 media exhibits an efficient degradation rate as complete removal of MG from solution was achieved within less than 16 min, indicating more than 50% increase in the rate of degradation which suggests the synthesized catalyst is of economic feasibility.

3.2.5. Effect of pH on degradation

pH is one of the key parameters that could affect the rate of degradation and adsorption as a preliminary step for the degradation using heterogeneous catalysis. In addition to its critical effect on the degradation processes in the liquid phase, it might result in some possible changes in the materials used depending on the nature of the degraded stuffs. The degradation of MG increases steadily with pH as shown in Fig. 8d. Complete degradation of the dye was recorded in less than 2 min for pH values 7 and 8. The degradation rate is maximum at alkaline pH = 8 decreasing gradually till it reaches minimum degradation at acidic pH = 3. Similar behavior was illustrated previously for cationic dyes [41]. The high photocatalytic activity in alkaline medium could be attributed to highly dispersive small sized particles which have more available active sites [21].

The high negative zeta potential values for the Si–HZnO in the alkaline medium indicates high stability and negatively charged structures as a result of oxygen atoms and/or hydroxyl groups on the catalyst surface. This suggests that strong donor–acceptor electrostatic and hydrophobic interactions are established between MG cationic dye and Si–HZnO [23]. Subsequently, such degradation processes are accompanied by the neutralization of the negative surface charge of the catalyst by the positively charged π–electron system of the dye, thus confirming the chemisorption as rate determining step and key factor in the degradation process [42].

3.2.6. Effect of ZnO loadings

Undoubtedly that the amount of loaded ZnO/$Zn(OH)_2$ and the doses used is one of the important parameters speeding the degradation rate of MG but not absolutely. Fig. 8e shows an enhancement in the degradation efficiency concurrently with the increase in catalyst dose varying from 0.05 to 0.25 g/100 mL of the dye. The results show 100% dye degradation at less than 2 min for a dose of 0.15 g/100 mL dye. Increasing dose than 0.15 g has a little effect on degradation. Upon these results 0.15 g/100 mL was selected for further experiments as the optimum dosage. Similar results have been reported in the literature [43].

3.2.7. Temperature effect on degradation process

Fig. 9 represents the data obtained upon investigating the effect of temperature within the range from 20°C to 35°C, on the degradation rate of MG using Si–HZnO photocatalyst. The rise in temperature showed a slight effect on the degradation rate with a maximum degradation rate observed at 35°C which reflects the endothermic nature of the degradation process of MG confirmed by the positive value of $\Delta H°$ recorded in Table 5. The complete disappearance of MG (50 mg L^{-1}) within less than 2 min can be revealed from the data. The value of the activation energy E_a associated with the complete decolorization of MG is calculated from the plot of ln K_{obs} vs. 1/T (Fig. 9), according to the Arrhenius equation:

$$\ln K_{obs} = \frac{-\Delta E_a}{RT} + \ln A \tag{12}$$

The value of E_a calculated from Arrhenius equation is 16.1 kJ.

The values of $\Delta S°$ and $\Delta H°$ can be calculated from the Eyring equation [41]. By plotting lnK_{obs}/T vs T in Fig. 9, a

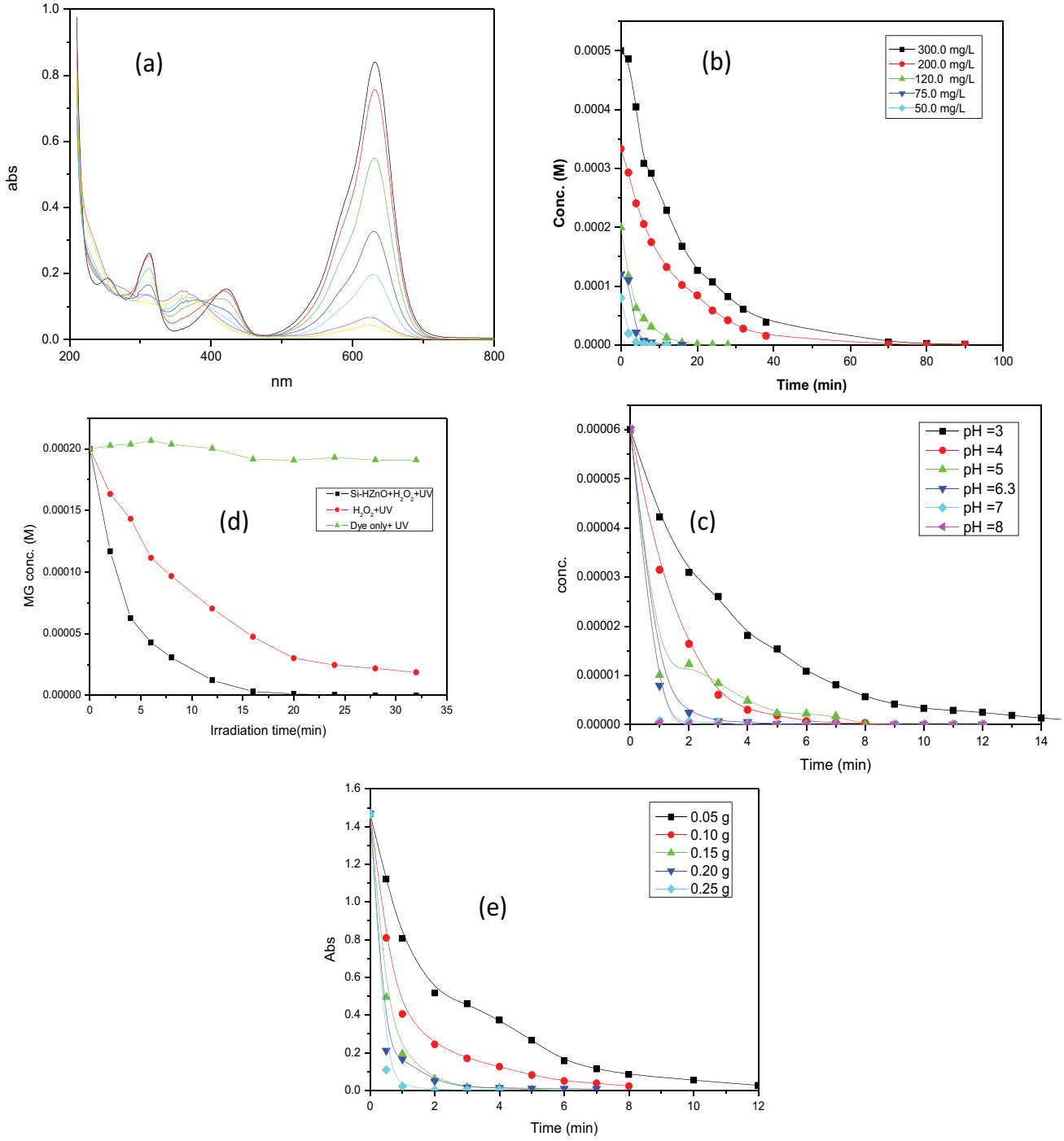

Fig. 8. (a) UV–Vis spectra of solution as a function of irradiation time (initial methyl green concentration: 120.0 mg L^{-1}). Photodegradation of MG: (b) different concentrations, (c) in presence of H_2O_2 only/H_2O_2 and Si–HZnO-II, (d) different pH and (e) different doses of Si–HZnO-II.

linear plot was observed from which $\Delta S°$ and $\Delta H°$ can be calculated. $\Delta G°$, the Gibb's free energy can be evaluated using Eq. (10). The spontaneous nature of the decolorization of the MG using Si–HZnO is indicated from the negative calculated values of $\Delta G°$ for the reaction (Table 5). The positive value of $\Delta S°$ recommends the increased randomness during the decolorization process.

3.2.8. Degradation kinetics

The experimental data of the photocatalytic process are illustrated by the pseudo-first-order kinetics simulation. As shown in Fig. 10, a plot of ln (C_0/C_t) against time of irradiation displays a straight line with linear correlation coefficient (R^2) equal to 0.997. It is obvious that all reactions

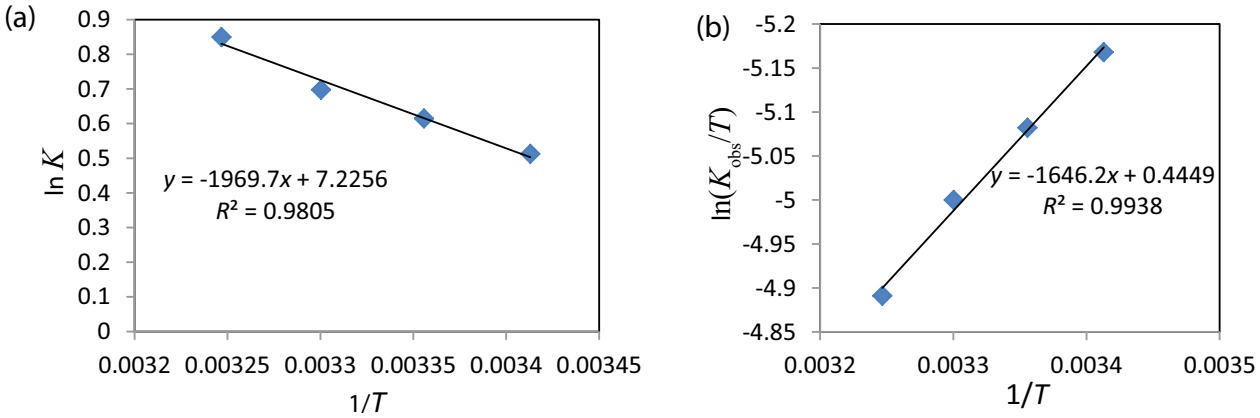

Fig. 9. (a) Plot of ln K vs. $1/T$ for the degradation process and (b) plot of ln (K_{obs}/T) vs. $1/T$ for degradation process.

Table 5
Calculated thermodynamic parameters for the effect of temperature on the degradation of MG using Si–HZnO

	Thermodynamic parameters						
Temperature	K_{obs} min^{-1}	ln K_{obs}	ln(K_{obs}/T)	$\Delta G°$ (kJ mol^{-1})	$\Delta H°$ (kJ mol^{-1})	$\Delta S°$ (J K^{-1} mol^{-1})	R^2
293	1.6996	0.513	–5.168	–1.249			
298	1.8492	0.615	–5.082	–1.523	14.31	53.13	0.991
303	2.035	0.678	–5.003	–1.707			
308	2.338	0.850	–4.881	–2.175			

follow first-order kinetics and the apparent rate constants calculated from the slopes of the straight lines indicate that the rate of degradation is directly proportional to the initial concentration of MG. Similar behavior has been reported for other photocatalysts [12].

3.3. Total organic carbon analysis

TOC analysis suggested that the products of the decolorization process are H_2O, CO_2, and NO_2. This could be confirmed from the measured parameters represented in Table 6 which indicated a steep decrease in the TOC and TC values. The nitrogen content of the dye disappeared, indicating the breaking of C=N bond in the dye. The presence of CO_2 is indicated by the increase in the IC content after degradation. Similar results were recorded in literature [44].

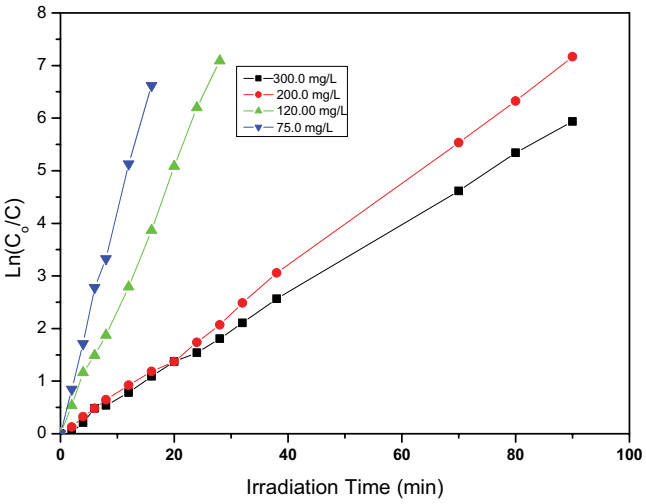

Fig. 10. ln (C_0/C) vs. time for the photodegradation of MG at different concentration of the dye.

3.4. Photocatalytic regeneration of Si–HZnO

At the end of degradation process, we noticed that the catalyst color was changed from white to blue due to adsorption of MG dye on it is surface. So, it is necessary to get rid of that dye in order to maintain the activity of the catalyst. There have been many attempts to reactivate the catalyst and the most successful is to expose the catalyst to 254 nm light source after a dip in 10 mL of solution containing 10 m H_2O_2. Complete decolorization and recovery of the exhausted catalyst was achieved after 5 min of illumination. The complete regeneration of the exhausted catalyst after degradation and adsorption of MG on its surface was successfully

Table 6
TOC parameters for MG before and after degradation

Parameter measured	MG dye before degradation (ppm)	MG dye after degradation (ppm)
TOC	22.64	0.659
TC	23.12	1.287
IC	0.4773	0.628
TN	2.024	0.000

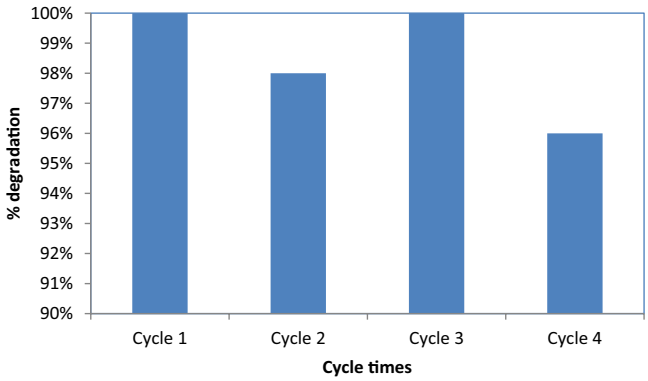

Fig. 11. Photodegradation of MG using Si–HZnO-II for four successive cycles.

accomplished and the catalyst color was turned white again and reused efficiently for four successive cycles (Fig. 11).

However, it was not the case for the SiO_2 sample saturated with the dye as its blue color did not alter; Since SiO_2 has no photocatalytic activity, it can only act as an adsorbent, and the adsorption capacity of SiO_2 saturated by MG cannot be photocatalytically recovered [4].

4. Conclusion

The current work indicates that although modification of silica gel with ZnO species could be utilized for the removal of MG dye via adsorption, the removal is achieved more efficiently through photodegradation. The results demonstrated that the ZnO species are well distributed inside the silicate matrix with average particle size lower than the detection limit of XRD. This distribution led to lowering the BET surface area due to the location of ZnO species in the silicate matrix. The data also reflect that the degradation process is pH and temperature dependent with increasing removal rate at higher pH and temperature values. Furthermore, the exhausted catalysts were exposed to successive regeneration and reuse. Future work will investigate the photocatalytic application of Si–HZnO in effluent water treatment in the presence of solar energy.

Acknowledgments

The authors are grateful to Research Units Labs, Faculty of Science, Imam Abdulrahman Bin Faisal University (IAU) for allowing the use and conducting most of the measurements of the research in its laboratories. Also, the authors would like to thank Dr. Hanadi B. Ahmed Baghdadi and all technicians in the research units for their support.

References

[1] L. Fan, C. Luo, M. Sun, X. Li, F. Lu, H. Qiu, Preparation of novel magnetic chitosan/graphene oxide composite as effective adsorbents toward methylene blue, Bioresour. Technol., 114 (2012) 703–706.
[2] Z. Aksu, Application of biosorption for the removal of organic pollutants: a review, Process Biochem., 40 (2005) 997–1026.
[3] M.A. Al-Ghouti, J. Li, Y. Salamh, N. Al-Laqtah, G. Walker, M.N.M. Ahmad, Adsorption mechanisms of removing heavy metals and dyes from aqueous solution using date pits solid adsorbent, J. Hazard. Mater., 176 (2010) 510–520.
[4] B. Jeong, D.H. Kim, E.J. Park, M.-G. Jeong, K.-D. Kim, H.O. Seo, Y.D. Kim, S. Uhm, ZnO shell on mesoporous silica by atomic layer deposition: removal of organic dye in water by an adsorbent and its photocatalytic regeneration, Appl. Surf. Sci., 307 (2014) 468–474.
[5] H.B. Hadjltaief, M.B. Zina, M.E. Galvez, P. Da Costa, Photocatalytic degradation of methyl green dye in aqueous solution over natural clay-supported ZnO–TiO_2 catalysts, J. Photochem. Photobiol., A, 315 (2016) 25–33.
[6] K. Nakata, A. Fujishima, TiO_2 photocatalysis: design and applications, J. Photochem. Photobiol., C, 13 (2012) 169–189.
[7] R. Saravanan, E. Thirumal, V.K. Gupta, V. Narayanan, A. Stephen, The photocatalytic activity of ZnO prepared by simple thermal decomposition method at various temperatures, J. Mol. Liq., 177 (2013) 394–401.
[8] P. Pourdayhimi, P.W. Koh, M. Mohd Salleh, H. Nur, S.L. Lee, Zinc oxide nanoparticles-immobilized mesoporous hollow silica spheres for photodegradation of sodium dodecylbenzenesulfonate, Aust. J. Chem., 69 (2016) 790–797.
[9] S. Gandhi, K. Thandavan, S. Sethuraman, U.M. Krishnan, Investigation of the photodegradation properties of iron oxide doped mesoporous SBA-15 silica, J. Porous Mater., 20 (2013) 1009–1015.
[10] M.M. El-Moselhy, A. Ates, A. Çelebi, Synthesis and characterization of hybrid iron oxide silicates for selective removal of arsenic oxyanions from contaminated water, J. Colloid Interface Sci., 488 (2017) 335–347.
[11] A.L. Rogach, A. Kornowski, M. Gao, A. Eychmüller, H. Weller, Synthesis and characterization of a size series of extremely small thiol-stabilized CdSe nanocrystals, J. Phys. Chem. B, 103 (1999) 3065–3069.
[12] M.M. El-Moselhy, N.M.R. Mahmoud, M.M. Emara, Copper modified exchanger for the photodegradation of methyl orange dye, Desal. Wat. Treat., 52 (2013) 7225–7234.
[13] M. Saadoun, B. Bessaïs, N. Mliki, M. Férid, H. Ezzaouia, R. Bennaceur, Formation of luminescent $(NH_4)_2SiF_6$ phase from vapour etching-based porous silicon, Appl. Surf. Sci., 210 (2003) 240–248.
[14] H. Kumar, A.K. Shukla, Fabrication Fe/Fe_3O_4/graphene nanocomposite electrode material for rechargeable Ni/Fe batteries in hybrid electric vehicles, Int. Lett. Chem. Phys. Astron., 19 (2013) 15–25.
[15] S. Fabbiyola, L.J. Kennedy, U. Aruldoss, M. Bououdina, A.A. Dakhel, J. Judithvijaya, Synthesis of Co-doped ZnO nanoparticles *via* co-precipitation: structural, optical and magnetic properties, Powder Technol., 286 (2015) 757–765.
[16] F. Tari, M. Shekarriz, S. Zarrinpashne, A. Ruzbehani, Modified and systematic synthesis of zinc oxide-silica composite nanoparticles with optimum surface area as a proper H_2S sorbent, Can. J. Chem. Eng., 95 (2016) 1632.
[17] K. Han, Z. Zhao, Z. Xiang, C. Wang, J. Zhang, B. Yang, The sol–gel preparation of ZnO/silica core–shell composites and hollow silica structure, Mater. Lett., 61 (2007) 363–368.
[18] V. Srikant, D.R. Clarke, On the optical band gap of zinc oxide, J. Appl. Phys., 83 (1998) 5447–5451.
[19] N. Kamarulzaman, M.F. Kasim, R. Rusdi, Band gap narrowing and widening of ZnO nanostructures and doped materials, Nanoscale Res. Lett., 10 (2015) 346.
[20] D. Attan, M.A. Alghoul, B.B. Saha, J. Assadeq, K. Sopian, The role of activated carbon fiber in adsorption cooling cycles, Renewable Sustainable Energy Rev., 15 (2011) 1708–1721.
[21] P. Sujaridworakun, K. Natrchalayuth, Influence of pH and HPC concentration on the synthesis of zinc oxide photocatalyst particle from zinc-dust waste by hydrothermal treatment, Adv. Powder Technol., 25 (2014) 1266–1272.
[22] H. Chun, W. Yizhong, H. Tang, Preparation and characterization of surface bond-conjugated TiO_2/SiO_2 and photocatalysis for azo dyes, Appl. Catal., B, 30 (2001) 277–285.
[23] Y. Kismir, A.Z. Aroguz, Adsorption characteristics of the hazardous dye Brilliant Green on Saklıkent mud, Chem. Eng. J., 172 (2011) 199–206.

[24] B. Kiran, A. Kaushik, Chromium binding capacity of *Lyngbya putealis* exopolysaccharides, Biochem. Eng. J., 38 (2008) 47–54.
[25] G. Crini, Non-conventional low-cost adsorbents for dye removal: a review, Bioresour. Technol., 97 (2006) 1061–1085.
[26] W. Weber, R.K. Chakravorti, Pore and solid diffusion models for fixed-bed adsorbers, Am. Inst. Chem. Eng. J., 20 (1974) 229–238.
[27] A. Sari, M. Tuzen, D. Citak, M. Soylak, Equilibrium, kinetic and thermodynamic studies of adsorption of Pb(II) from aqueous solution onto Turkish kaolinite clay, J. Hazard. Mater., 149 (2007) 283–291.
[28] M. Bahgat, A.A. Farghali, W. El Rouby, M. Khedr, M.Y. Mohassab-Ahmed, Adsorption of methyl green dye onto multi-walled carbon nanotubes decorated with Ni nanoferrite, Appl. Nanosci., 3 (2013) 251–261.
[29] N.M. Bandaru, N. Reta, H. Dalal, A.V. Ellis, J. Shapter, N.H. Voelcker, Enhanced adsorption of mercury ions on thiol derivatized single wall carbon nanotubes, J. Hazard. Mater., 261 (2013) 534–541.
[30] H. Kaygusuz, S. Uzaşçı, F.B. Erim, Removal of fluoride from aqueous solution using aluminum alginate beads, Clean Soil Air Water, 43 (2015) 724–730.
[31] R.-L. Tseng, F.-C. Wu, Inferring the favorable adsorption level and the concurrent multi-stage process with the Freundlich constant, J. Hazard. Mater., 155 (2008) 277–287.
[32] M. Hosseini, S.F.L. Mertens, M. Ghorbani, M.R. Arshadi, Asymmetrical Schiff bases as inhibitors of mild steel corrosion in sulphuric acid media, Mater. Chem. Phys., 78 (2003) 800–808.
[33] A.O. Dada, A.P. Olalekan, A.M. Olatunya, O. Dada, Langmuir, Freundlich, Temkin and Dubinin–Radushkevich isotherms studies of equilibrium sorption of Zn^{2+} unto phosphoric acid modified rice husk, IOSR J. Appl. Chem., 3 (2012) 38–45.
[34] X.-j. Hu, J.-s. Wang, Y.-g. Liu, X. Li, G.-m. Zeng, Z.-l. Bao, X.-x. Zeng, A.-w. Chen, F. Long, Adsorption of chromium (VI) by ethylenediamine-modified cross-linked magnetic chitosan resin: isotherms, kinetics and thermodynamics, J. Hazard. Mater., 185 (2011) 306–314.
[35] S. Gupta, B.V. Babu, Utilization of waste product (tamarind seeds) for the removal of Cr(VI) from aqueous solutions: equilibrium, kinetics, and regeneration studies, J. Environ. Manage., 90 (2009) 3013–3022.
[36] B.H. Hameed, D.K. Mahmoud, A.L. Ahmad, Equilibrium modeling and kinetic studies on the adsorption of basic dye by a low-cost adsorbent: coconut (*Cocos nucifera*) bunch waste, J. Hazard. Mater., 158 (2008) 65–72.
[37] M. Roulia, A.A. Vassiliadis, Sorption characterization of a cationic dye retained by clays and perlite, Microporous Mesoporous Mater., 116 (2008) 732–740.
[38] M. Ghaedi, J. Tashkhourian, A.A. Pebdani, B. Sadeghian, F.N. Ana, Equilibrium, kinetic and thermodynamic study of removal of reactive orange 12 on platinum nanoparticle loaded on activated carbon as novel adsorbent, Korean J. Chem. Eng., 28 (2011) 2255–2261.
[39] M.M.R. Emara, A.A. Salman, N.M.R. Mahmoud, S.A. Fattah, Removal of fluoride from aqueous solution using Amberlite-IRA-aluminum sorbent nanoexchanger, Desal. Wat. Treat., 81 (2017) 152–161.
[40] H. Genç-Fuhrman, J.C. Tjell, D. McConchie, Adsorption of arsenic from water using activated neutralized red mud, Environ. Sci. Technol., 38 (2004) 2428–2434.
[41] M.M. El-Moselhy, Methylene blue dye degradation using C-100 polymeric material modified with ZnO nanoparticles, Desal. Water Treat., 57 (2016) 25800–25811.
[42] E.A. Rogozea, A. Meghea, N.L. Olteanu, A. Bors, M. Mihaly, Fullerene-modified silica materials designed for highly efficient dyes photodegradation, Mater. Lett., 151 (2015) 119–121.
[43] N.S.F. Trotte, M. Alzamora, D.R. Sánchez, N.M.F. Carvalho, Removal of methyl orange by heterogeneous Fenton catalysts prepared using glycerol as green reducing agent, Environ. Technol., 39 (2018) 2822–2833.
[44] M.-C. Chang, H.-Y. Shu, T.-H. Tseng, H.-W. Hsu, Supported zinc oxide photocatalyst for decolorization and mineralization of Orange G dye wastewater under UV365 irradiation, Int. J. Photoenergy., 2013 (2013) 1–12.